

Defining an equivalent homogeneous roughness length for turbulent boundary layers developing over patchy or heterogeneous surfaces.

N Hutchins^{a,*}, B Ganapathisubramani^b, MP Schultz^c and DI Pullin^d

^aDepartment of Mechanical Engineering, The University of Melbourne, Victoria 3010, Australia

^bAerodynamics and Flight Mechanics Research Group, University of Southampton, Southampton SO17 1BJ, UK

^cDepartment of Naval Architecture & Ocean Engineering, US Naval Academy, Annapolis, MD21402-5042, USA

^dGraduate Aerospace Laboratories, California Institute of Technology, Pasadena, California 91125, USA

ARTICLE INFO

Keywords:

heterogeneous roughness
rough wall bounded turbulence
biofouling
hull roughness

ABSTRACT


A new approach based on the power mean is suggested for defining an equivalent homogeneous roughness length k_{ehr} which takes into account patchiness or heterogeneous distribution of roughness on ship hulls and can be readily incorporated into existing full-scale drag prediction methods. In the limit where patch sizes are much greater than the boundary layer thickness, it is readily shown that the relationship between drag coefficient and roughness length is non-linear, highlighting an obvious source of error with current approaches that attempt to define an equivalent homogeneous roughness through an area-weighted arithmetic mean. The degree of error is dependent on the roughness distribution, but is estimated to exceed 16% for highly skewed beta heterogeneous distributions. For fully-rough models, the power mean approach returns errors of $< 1\%$ for the distributions tested here. The efficacy of the power mean approach is also evaluated in the transitional regime and with different transitional roughness models (Nikuradse and Colebrook) and retains accuracy for most realistic operating scenarios.

1. Introduction

Many full-scale predictions of the drag penalty due to surface roughness for wall-bounded turbulence rely on ascribing an assumed homogeneous equivalent sandgrain roughness k_s , or other equivalent quantity (for example z_0 for atmospheric flows). In the fully-rough regime, one can use k_s to predict the downwards shift in the viscous scaled mean velocity profile (ΔU^+ , the Hama roughness function) using $\Delta U^+ = \kappa^{-1} \ln k_s^+ + A - B$, where κ , A and B are assumed empirical constants ($\kappa \approx 0.4$ is the von Kármán constant, $A \approx 5$ is the smooth wall intercept for the log law and $B \approx 8.5$ is Nikuradse's 1933 fully rough intercept for uniform sand grains). The superscript $+$ here denotes viscous scaling (i.e. $k_s^+ = k_s U_\tau / \nu$ or $U^+ = U / U_\tau$, where U_τ is the local wall friction velocity and ν is the kinematic viscosity). The value for the roughness function ΔU^+ can in turn be related to the local frictional drag for the rough surface C_{fr} . For fully-developed internal flows, such as channels and pipe flows, this is straight-forward and given by

$$\sqrt{\frac{2}{C_{fs}}} - \sqrt{\frac{2}{C_{fr}}} = \Delta U^+, \quad (1)$$

where C_{fs} and C_{fr} are the drag coefficients for the smooth and rough surfaces respectively at matched friction Reynolds numbers $Re_\tau (\equiv \delta U_\tau / \nu = \delta^+$, where δ is the boundary layer thickness). The drag coefficient is defined here relative to the centerline velocity U_∞ , such that $C_f \equiv 2\tau_w / \rho U_\infty^2 = 2U_\tau^2 / U_\infty^2 = 2/U_\infty^{+2}$, where τ_w is the wall shear stress and ρ is density. For evolving turbulent boundary layers, equation (1) is less useful, since the ratio of k_s to the boundary layer thickness δ , and hence C_f is a function of streamwise distance x along the plate. In this case, the von Kármán momentum integral equation must be used to solve for the streamwise evolution (see for example Prandtl and Schlichting, 1934; Granville, 1958; Monty, Dogan, Hanson, Scardino, Ganapathisubramani and Hutchins, 2016; Pullin, Hutchins and Chung, 2017; Chung, Hutchins, Schultz and Flack, 2021) and the streamwise developing local skin friction coefficient C_f must be integrated along the length of the plate to obtain the drag penalty (see equation 2).

 nhu@unimelb.edu.au (N. Hutchins)

ORCID(S): 0000-0001-7511-2910 (N. Hutchins)

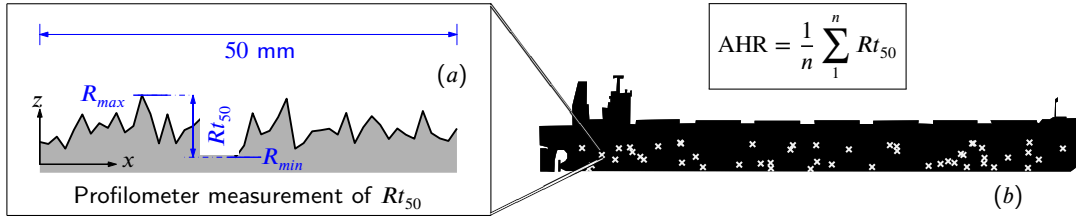


Figure 1: Illustration of the current method of measuring average hull roughness (AHR)

Though the methods discussed above are able to predict drag penalties for evenly distributed roughness, such an idealised configuration is rarely encountered in practise. The roughness due to biofouling on ship hulls can be highly non-homogeneous or patchy. This poses the problem of how heterogeneity can be incorporated into low order predictive models such as those discussed above. The cases of streamwise and spanwise heterogeneity have been studied in isolation in seminal works by Antonia and Luxton (1971, 1972) and Hinze (1967) respectively, to name but a few. Even for these idealised cases, the results demonstrate a rich physics that will pose problems for predictive models. In the case of streamwise (x) variation, it is noted that following a change in surface condition, the developing internal layer takes a considerable streamwise distance to recover fully to equilibrium with the new surface condition. Antonia and Luxton (1971, 1972); Saito and Pullin (2014); Hanson and Ganapathisubramani (2016); Rouhi, Chung and Hutchins (2019); Li, de Silva, Chung, Pullin, Marusic and Hutchins (2021) all show that following a streamwise change in surface condition there can be over- or under-shoots in local C_f (for rough-to-less-rough or rough-to-more-rough transitions, respectively) relative to the equilibrium value. For spanwise heterogeneity it is noted that the presence of secondary flows, located close to the spanwise transitions in wall roughness condition, cause local non-equilibrium behaviour (Yang and Anderson, 2018; Chung, Monty and Hutchins, 2018; Medjnoun, Vanderwel and Ganapathisubramani, 2018; Wangsawijaya, Baidya, Chung, Marusic and Hutchins, 2020). For cases where the spanwise wavelength of the heterogeneity is $\approx \delta$, these secondary flows become space filling and subsequently such flows lose all equilibrium behaviour (and cease to obey Townsend's 1976 outer layer similarity).

Presently, in maritime applications, low-order models that attempt to deal with heterogeneity ascribe an equivalent homogeneous roughness length by taking the arithmetic mean of roughness observations. For example, during dry-dock, hull roughness is typically quantified via profilometer measurements of the peak-to-trough roughness height over a 50 mm traverse, Rt_{50} (see Fig. 1a). This process is repeated at many locations over the hull of the vessel and the average hull roughness AHR is defined as the arithmetic mean of all observed Rt_{50} (see Fig. 1b), which subsequently provides the input into hull drag penalty calculations (International Paints, 2004). The averaging process here is designed to account for heterogeneity. If in-water dive inspections are used, a similar (though more subjective) averaging process is performed, with divers ascribing a fouling scale and percentage coverage based on observations (see for example Naval Ships' Technical Manual, 2006). Again, just like AHR, this will provide an equivalent homogeneous roughness lengthscale that can be used as an input into low order drag predictions. There are two significant problems represented by the averaging suggested in Fig. 1. Firstly, this approach has the implicit assumption that the dynamic effect of the surface roughness on the flow can be entirely accounted for through a single topographical parameter, the peak-to-trough roughness height k_r . In reality, it is known that the dynamic effect of the surface on the flow and drag (which is embodied in the equivalent sandgrain roughness k_s) depends on many parameters, which in addition to a measure of height will likely include some measure of frontal solidity or effective slope (Schlichting, 1936; Napoli, Armenio and De Marchis, 2008; Raupach, Antonia and Rajagopalan, 1991; Chan, MacDonald, Chung, Hutchins and Ooi, 2015) and a measure of plan solidity or skewness (Placidi and Ganapathisubramani, 2015; Macdonald, Griffiths and Hall, 1998; Flack and Schultz, 2010; Jelly and Busse, 2018; Flack, Schultz and Barros, 2020). Many other parameters have also been suggested (Thakkar, Busse and Sandham, 2017; Busse and Jelly, 2020; Chung et al., 2021). Secondly, the averaging process depicted in Fig. 1 suggests that, from a low-order approach, a simple area-weighted arithmetic mean of the roughness is sufficient to account for heterogeneity. In this study we will deal solely with the latter problem. The former, the ability to ascribe an equivalent sandgrain roughness based on topographical observations, is a work in progress and the focus of much ongoing research (Chung et al., 2021; Flack and Chung, 2022), but will be assumed throughout this study. In this manner, we will isolate the heterogeneity problem.

To appreciate the issue with the arithmetic mean approach of Fig. 1 and also to introduce our proposed solution,

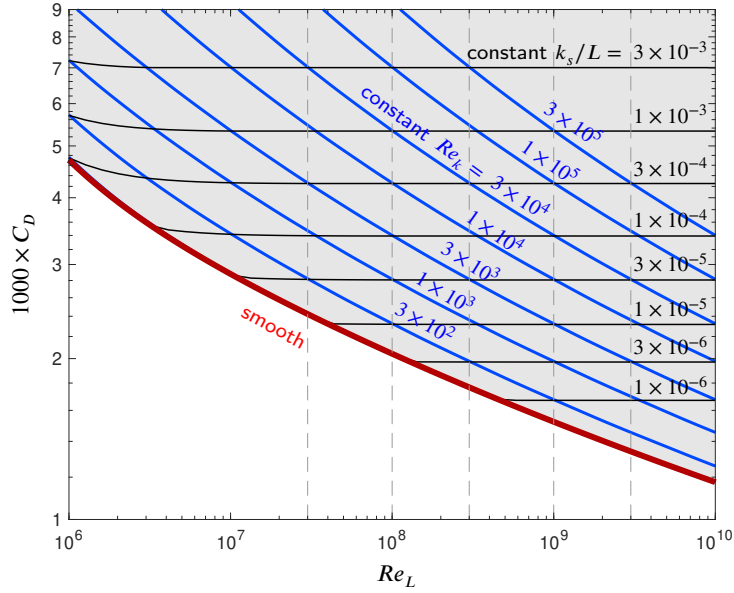


Figure 2: Integrated drag (C_D) over a flat plate of length L for various (—) roughness Reynolds numbers Re_k and (—) ratios k_s/L . These calculations follow the methodology of Monty et al. (2016) and Pullin et al. (2017) and assume $\kappa = 0.4$, $B_{s\infty} = 8.5$, and the wake function and parameters as given in Monty et al. (2016).

consider Fig. 2 which shows the plate-integrated friction drag C_D as a function of Reynolds number for a plate of length L . Here $Re_L \equiv LU_\infty/\nu$ is the Reynolds number based on plate length, where U_∞ is the freestream velocity (or speed of the ship). The black and blue curves show different roughness scenarios; constant k_s/L and constant Re_k ($\equiv k_s U_\infty/\nu$) respectively. The red curve shows the smooth plate result. Here the plate integrated drag is defined as

$$C_D = \frac{1}{L} \int_{x=0}^L C_f dx. \quad (2)$$

Fig. 2 is calculated using the methodology outlined in Monty et al. (2016) and Pullin et al. (2017). Fully-rough behaviour is assumed for all k_s^+ , for which the Hama roughness function ΔU^+ is defined as,

$$\Delta U^+ = \begin{cases} \frac{1}{\kappa} \log k_s^+ + A - B, & \text{if } k_s^+ \geq e^{\kappa(B-A)} \\ 0, & \text{otherwise.} \end{cases} \quad (3)$$

The ramifications of more complex expressions for $\Delta U^+(k_s^+)$ will be explored later (§ 4.2). Fig. 3 shows drag coefficient against k_s/L for the five Re_L shown by the dashed lines in Fig. 2. Note that under this scaling, and in the fully rough regime, drag curves for all Re_L collapse to the same curve. The pink shaded region of Fig. 3 shows the smooth regime, which for the roughness function described by equation 3 corresponds to $k_s^* \lesssim e^{\kappa(B-A)}$. Here $k_s^* = kU_\tau^*/\nu$ is defined on the plate integrated drag where $U_\tau^* = U_\infty \sqrt{C_D/2}$. It is evident that in this regime the drag curves depart from the fully-rough asymptote and become invariant with k_s/L (since $\Delta U^+ = 0$). These are the horizontal black lines in Fig. 3, which can be understood by considering the point where the dashed vertical lines in Fig. 2 meet the smooth drag curve (shown in red). Lines of constant Re_k are shown by the blue curves in Fig. 3 (note that, $Re_k = \frac{k_s}{L} Re_L$). Although, strictly speaking, the locus between the fully rough and smooth regimes is $k_s^* = e^{\kappa(B-A)}$, it is seen that for the range of Re_L and k_s/L considered in Fig. 3 (which is designed to be encompassing of most ship operations) a curve of constant Re_k (≈ 150) approximately describes this transition. All curves for $Re_k > 150$ lie on the fully rough asymptote. This can be explained since, $k_s^* = Re_k \sqrt{C_D/2}$, and hence for the range of Re_L considered in Fig. 3, $k_s^* = e^{\kappa(B-A)}$ corresponds to $116 < Re_k < 156$ for the considered Reynolds number range $3 \times 10^7 < Re_L < 3 \times 10^9$.

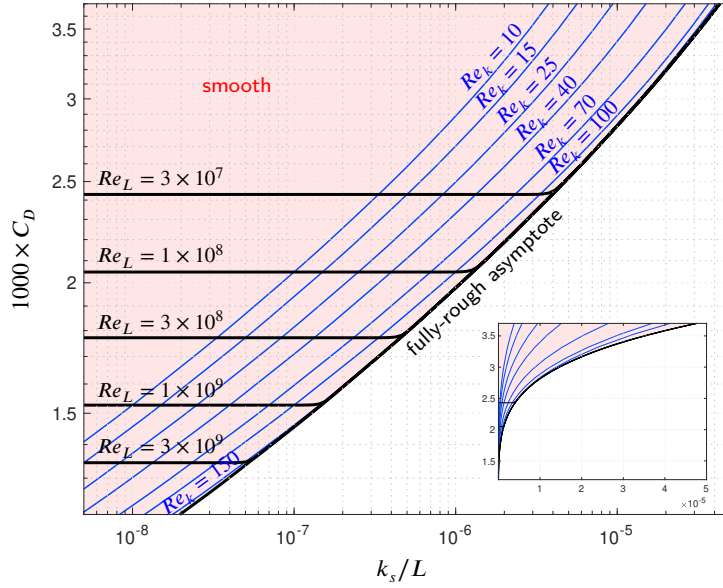


Figure 3: Integrated drag (C_D) over a flat plate of length L as a function of k_s/L for various (—) roughness Reynolds numbers Re_k and (— for the plate Reynolds numbers Re_L as indicated by the dot-dashed lines in Fig. 2). These calculations follow the methodology of Monty et al. (2016) and Pullin et al. (2017) and assume $\kappa = 0.4$, $B_{s\infty} = 8.5$, and the wake function and parameters as given in Monty et al. (2016). The red shaded region shows the smooth wall behaviour, the black constant Re_L curves all collapse to a fully rough asymptote. The Hama roughness function is here assumed to be fully rough $\Delta U^+ = \kappa^{-1} \log k_s^+ + A - B$ for $k_s^+ \geq e^{\kappa(B-A)}$ and otherwise $\Delta U^+ = 0$ (as defined in equation 3). The inset shows a version of this figure with linear axes.

2. Power-Law modelling

In terms of roughness heterogeneity, the most important attribute of Fig. 3 is that in the fully rough regime C_D is only a function of k_s/L (Reynolds number invariance) and also that C_D varies non-linearly with k_s (see the inset of Fig. 3 which shows the same data plotted on linear axes). In the fully rough regime, the relationship between C_D and k_s/L is fairly well described by the power law,

$$C_D \propto (k_s/L)^n \quad (4)$$

Though imperfect, such a power law approximation is attractive since it permits us to define an equivalent homogeneous roughness (k_{ehr}) based on an area weighted power mean of the heterogeneous roughness observations. Here k_{ehr} is defined as an equivalent roughness length for which a homogeneous coverage will yield the same overall drag characteristics as a given observed heterogeneous distribution. Given N patches of roughness with area A_i , equivalent sandgrain roughness length k_{si} and drag coefficient C_{Di} , the total observed drag of the vessel will be given by

$$C_D = \frac{1}{A} \sum_{i=1}^N C_{Di} A_i \quad \text{where} \quad A = \sum_{i=1}^N A_i. \quad (5)$$

For simple two-patch configurations in tow-tank experiments, Song, Ravenna, Dai, DeMarco Muscat-Fenech, Tani, Demirel, Atlar, Day and Incecik (2021) have recently shown that equation (5) is valid even when C_{Di} (the drag of the i th patch) is replaced with the drag predicted using Granville's (1958) method for a homogeneous distribution of the i th patch roughness k_{si} over the entire hull. This is analogous to replacing the patch roughness drag coefficient C_{Di} in

equation (5) with the power law from equation(4), suggesting that,

$$C_D \propto \frac{1}{A} \sum_{i=1}^N \left(\frac{k_{si}}{L} \right)^n A_i. \quad (6)$$

The purpose of an equivalent homogeneous roughness k_{ehr} would be to avoid the summation in (6), and instead represent the distribution with a single roughness length

$$C_D \propto \left(\frac{k_{ehr}}{L} \right)^n. \quad (7)$$

Equating (6) and (7) would suggest that the equivalent homogeneous roughness length could be defined by the following power mean

$$k_{ehr} = \left[\frac{1}{A} \sum_{i=1}^N k_{si}^n A_i \right]^{\frac{1}{n}}. \quad (8)$$

Note that the constant of proportionality inherent in equation (4) does not influence this approximation¹. Equation (8) can be compared to the current practise of taking the arithmetic mean (implied by the use of the average hull roughness AHR, see Fig. 1)

$$k_{ahr} = \frac{1}{A} \sum_{i=1}^N k_{si} A_i. \quad (11)$$

Note that k_{ahr} , the area-weighted arithmetic mean of k_{si} , could only yield the correct estimate for the drag if $n = 1$. The inset of Fig. 3 shows that this implied linearity does not exist.

As a cautionary note, the methods used to produce Fig. 3 (Prandtl and Schlichting, 1934; Granville, 1958; Monty et al., 2016; Pullin et al., 2017; Chung et al., 2021) implicitly assume that the local boundary layer is predominantly in equilibrium with the local surface conditions. Since the power mean approximation of equation (8) is extracted from these equilibrium calculations, we must add the caveat that the power mean is only expected to be correct in the limit where $A_i \gg \delta_i^2$ (where δ_i is the local boundary layer thickness). Secondary flows and internal layers will exist close to the transitions in roughness length, and these regions, which could be $O(\delta)$ in the span (see Wangsawijaya et al. 2020) and $O(10\delta)$ in the streamwise direction (see Li et al., 2021), will have local drag coefficients that do not match (are not in equilibrium with) the local surface condition. The current study sidesteps this issue by considering heterogeneous scenarios where the strips (of length L) extend the entire length of the vessel (see figure 4). Not only does this avoid any required front-to-back weighting for patch location, but also minimises the effect of the equilibrium assumption (provided the strip widths can be considered to be $\gg \delta$, which is the case for the scenarios analysed here). As justification for this approach, studies by Suastika, Hakim, Nugroho, Nasirudin, Utama, Monty and Ganapathisubramani (2021) and Song et al. (2021) suggest that the front-to-back ordering of heterogeneous patches is of secondary importance, causing only minor changes in the integrated drag coefficient C_D . In the future, it may be the case that a measure of streamwise patch location \hat{x} could be incorporated into the power mean approach (perhaps as a weighting parameter, or as a normalising lengthscale for k). For now, however, we stick to the approach implied by equation (8).

Previously, there have been attempts to analytically ascribe an equivalent homogeneous roughness length based on the assumed logarithmic form of the mean velocity profile for a flow in equilibrium with a local patch of roughness. Such attempts are prevalent in the atmospheric boundary layer literature, often pertaining to large eddy simulations

¹Equation (4) implies that $C_{Di} = a + b(k_s/L)^n$, where a and b are constants. For a simple two patch scenario, equation (5) would suggest that,

$$C_D = \frac{1}{A} \left[A_1 \left(a + b \left(\frac{k_{s1}}{L} \right)^n \right) + A_2 \left(a + b \left(\frac{k_{s2}}{L} \right)^n \right) \right] = a + \frac{b}{A} \left[A_1 \left(\frac{k_{s1}}{L} \right)^n + A_2 \left(\frac{k_{s2}}{L} \right)^n \right], \quad (9)$$

using equation (8) suggests that,

$$C_D = a + b \left(\frac{k_{ehr}}{L} \right)^n. \quad (10)$$

(LES). Many different approaches exist, the simplest of which (see for example Taylor, 1987) assumes that an equivalent roughness can be given by an area weighted geometric mean

$$\ln z_{0,ehr} = \frac{1}{A} \sum_{i=1}^N (\ln z_{0i}) A_i, \quad (12)$$

where z_0 is the roughness length (related to k_s via $z_0 = k_s \exp[-\kappa B]$). Here $z_{0,ehr}$ is an equivalent homogeneous roughness length that will return the space averaged logarithmic mean velocity profile and z_{0i} is the roughness length over the individual heterogeneous patches. This approach essentially assumes that the wall shear stress does not vary for different roughness patches, which is not a suitable assumption for developing turbulent boundary layers. Other attempts have started with the assumption that the total wall shear stress over a heterogeneous domain can be written as the area average of the local wall shear stress for each patch within the domain, similar to equation (5). From this assumption, and again assuming local logarithmic velocity profiles, it has been variously shown (see Bou-Zeid, Meneveau and Parlange, 2004, for example) that if the velocity at the co-called ‘blending height’ z_b is invariant with the local roughness condition, then the equivalent homogeneous roughness length is given by the following

$$\left(\ln \frac{z_b}{z_{0,ehr}} \right)^{-2} = \frac{1}{A} \sum_{i=1}^N A_i \left(\ln \frac{z_b}{z_{0i}} \right)^{-2}. \quad (13)$$

This approach, when coupled with a semi-empirical relationship for the blending height (the height beyond which internal boundary layers due to individual roughness patches merge to give spatially uniform velocity), permits calculation of $z_{0,ehr}$ (Bou-Zeid et al., 2004). For developing turbulent boundary layers however, the concept of a blending height is questionable since the mean velocity U at fixed height z develops indefinitely with streamwise location x . Additionally, for scenarios where the heterogeneous patch size is $\gg \delta$, the blending height would only occur at the boundary layer edge $z_b = \delta$. Hence these semi-analytical approaches based on assumed logarithmic profiles would be unlikely to succeed. Indeed, Pullin et al. (2017) shows that the relationship between plate integrated drag and k_s for a developing flat plate boundary layer is much more complicated than the simple logarithmic forms assumed for the atmospheric surface layer. Ultimately, an analytical approach for developing turbulent boundary layers is unlikely to yield a practical definition for equivalent homogeneous roughness length.

Based on the premise that the power mean suggested by (8) may provide a suitable approach for defining an equivalent homogeneous roughness length, this paper sets about defining a suitable exponent n , and then tests the efficacy of this proposed power mean averaging using the predictive methods proposed by Granville (1958); Monty et al. (2016); Pullin et al. (2017). The influence of different roughness distributions is explored, along with refinements required to cope with heterogeneous distributions that extend into the transitional regime.

3. Testing the proposed expression for k_{ehr} (equation 8)

The proposed expression for the equivalent homogeneous roughness k_{ehr} is tested by modeling a flat plate covered by N spanwise strips of different roughness heights over the width of the plate W (see Fig. 4). Provided that we assume the strip width $W/N \gg \delta$, we can neglect the effect of the secondary flows that will form at the strip boundaries. These N strips will form a random distribution of roughness heights between some lower and upper limits, defined as k_{s1} and k_{s2} respectively. To define the lower limit, we for now restrict analyses to the fully rough regime where $k_{s1}^* = e^{\kappa(B-A)}$, which as explained above suggests that $Re_{k_{s1}} \approx 150$. For the upper limit, we choose the value suggested by Schultz (2007) of $k_{s2} = 0.01$ m for heavy calcareous fouling. The roughness length for each strip, k_{si} , where $i = 1:N$, is uniformly distributed within the range $k_{s1} < k_{si} < k_{s2}$

$$\frac{150\nu}{U_\infty} < k_{si} < 0.01\text{m}. \quad (14)$$

These limits are selected to be somewhat realistic for shipping applications. For the vessel investigated by Schultz (2007), $Re_{k_{s1}} = 150$ corresponds to $k_{s1} \approx 15\mu\text{m}$, which is approximately half of the tabulated roughness height for an as-applied anti-fouling coating listed in that study. Hull roughness observations will occasionally be made that lie beyond this range. The case where $k_{s1} < 150\nu/U_\infty$ is investigated in § 4. For now, we use the predictive boundary layer evolution methodologies outlined in Granville (1958); Monty et al. (2016); Pullin et al. (2017) to estimate the drag coefficient C_D for each of the N strips on the modeled flat plate shown in Fig. 4 with the roughness

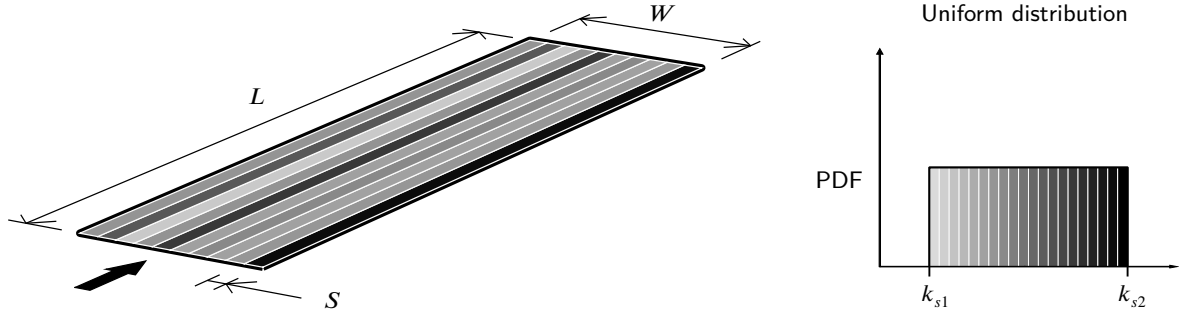


Figure 4: A flat plate of length L and width W , comprised of N strips of different roughness, where the strip width $S = W/N$ and the roughness of each strip k_s is taken from a uniform distribution.

distributions as described in (14). The predictive evolution methodologies will provide C_{Di} which in turn, via (5), permits an estimate of the total drag coefficient C_D due to the heterogeneous roughness. This is considered the true estimate, since the equilibrium assumption embedded in these predictive methodologies is reasonable in the limit of $A_i \gg \delta^2$ ($W/N \gg \delta$). This true or ‘correct’ result is then compared to the estimate based on an equivalent homogeneous roughness k_{ehr} . The value for k_{ehr} , calculated from (4) for the assumed roughness distribution, gives a single homogeneous roughness input to a similar calculation (using methodologies outlined in Granville, 1958; Monty et al., 2016; Pullin et al., 2017) to yield a value for $C_{D_{ehr}}$ (the drag estimate based on an assumed homogeneous roughness k_{ehr}).

We test this for a flat-plate with $N = 10$ (10 spanwise strips as illustrated in Fig. 4), and in the Reynolds number range $3 \times 10^7 < Re_L < 1 \times 10^{10}$. Since we set $k_{s2} = 0.01$ mm (a dimensional value), we make the problem dimensionless by considering a range of plate lengths from $1 < L < 300$. These encompass the limits of ship operations, and permit us to define a range of k_{s2}/L .

3.1. The optimal power n

First we test the scenario described above to determine n_{opt} , the optimal power n to minimise the error in $C_{D_{ehr}}$. For each (Re_L, L) combination we compute the optimal n , by minimising the error between C_D (the true estimate of the plate integrated drag) and the estimate based on the equivalent homogeneous roughness k_{ehr}

$$n_{opt} = \arg \min |(C_D - C_{D_{ehr}})|. \quad (15)$$

Since the roughness length for each of the N strips is randomly assigned from a uniform distribution within the limits given by (14), a total of 100 repeated calculations are performed to obtain statistical convergence. Fig. 5(a) shows n_{opt} as a function of Re_L and \bar{k}/L , where \bar{k} is the arithmetic mean roughness height from the distribution ($\bar{k} = (k_{s1} + k_{s2})/2$ for a uniform distribution). The symbol shading shows Re_L , from lowest (lightest) to highest (darkest shading). The rhombus symbols show the case where $k_{s2} = 0.01$ m, while the filled circle symbols show $k_{s2} = 0.001$ m. As can be seen, all data collapse reasonably well, regardless of Re_L and k_{s2} , onto a single curve of the form

$$n_{opt} = c \left(\frac{k_{s2}}{L} \right)^d, \quad (16)$$

with Fig. 5(a) suggesting $c = 0.516$ and $d = 0.0818$. The range of \bar{k}/L shown in Fig. 5(a) represents extreme operating conditions. Coupled with the low value for d , this suggests that a reasonable estimate for k_{ehr} and $C_{D_{ehr}}$ can be obtained with a fixed value of n . As an example, based on the fit given in equation (16), a \pm one decade variation in \bar{k}/L (indicated by the shaded region in figure 5a) will yield a variation in n_{opt} of ± 0.05 . It can be shown that such variations have only moderate effect on the accuracy of the power mean approach. Fig. 5(b) shows the percentage

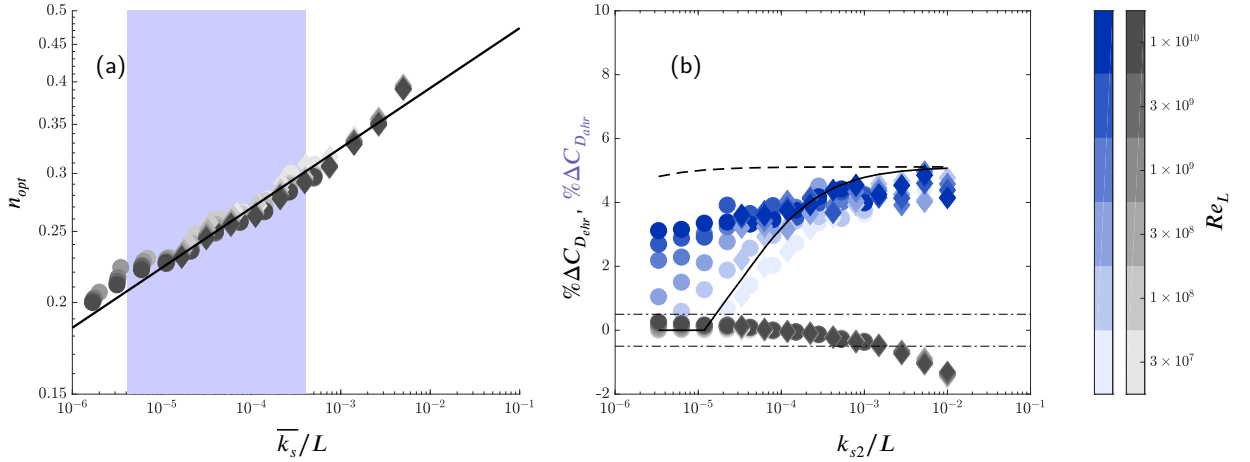


Figure 5: (a) The optimal power n_{opt} as a function of \bar{k}_s/L and Re_L for the uniform distribution. The solid line shows $n_{opt} = A(\bar{k}_s/L)^B$ with $A = 0.57$ and $B = 0.081$. The symbol size corresponds to ± 2 standard deviations for the computed n_{opt} between the 100 runs. (b) Shows a case with $n = 0.25$, showing the percentage error (grey shaded symbols) between the drag predictions using the power mean k_{ehr} and the true estimate of the drag ($\Delta C_{D_{ehr}} = C_{D_{ehr}} - C_D$) and (blue shaded symbols) between the drag predictions using the arithmetic mean k_{ahr} and the true estimate of the drag ($\Delta C_{D_{ahr}} = C_{D_{ahr}} - C_D$). The (o) symbols show data with $k_{s2} = 0.001$ m and the (\diamond) symbols show $k_{s2} = 0.01$ m. The colour shading shows Re_L , with darkest shading showing highest Re_L (see colour scales on right-hand side). The dot-dashed lines in plot (b) show a $\pm 0.5\%$ margin, the solid and dashed lines show the predicted error from the PDF (equation 18) evaluated at $Re_L = 3 \times 10^7$ and $Re_L = 1 \times 10^{10}$.

error in $C_{D_{ehr}}$ (grey shaded symbols) and $C_{D_{ahr}}$ (blue shaded symbols) as compared to the true estimate C_D , where the power mean k_{ehr} is computed using a fixed exponent $n = 0.25$. Clearly the error due to the estimate based on the power mean is lower than that due to the arithmetic mean ($n = 1$). At very low Reynolds numbers, and low k_{s2}/L , the error due to the arithmetic mean is minimal. This is expected since k_{s2} is very close to k_{s1} , and hence the non linearity observed in Fig. 3 is less of an issue. However, as Re_L increases (darker shaded symbols) and as k_{s2}/L increases, the error in taking the arithmetic mean increases. The error due to assuming $n = 0.25$ for the power mean approach remains $< 0.5\%$ for $k_{s2}/L < 10^{-3}$, this corresponds to the \bar{k}/L range shaded blue in Fig. 5(a), suggesting that for most ship operations we might avoid the complication of equation (16) and instead assume a constant $n \approx 0.25$.

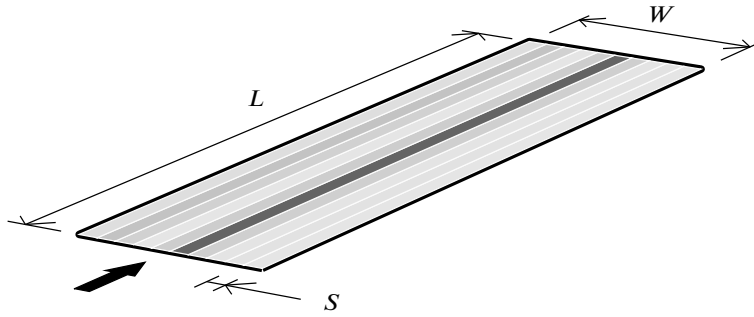
The behaviour shown in Fig. 5(b) can be predicted based on the assumed probability distribution and equations (7) - (11). For a uniform probability distribution function $P(k) = 1/(k_{s2} - k_{s1})$, we can write that

$$\bar{k}^n = \int_{k_{s1}}^{k_{s2}} k^n P(k) dk = \frac{k_{s2}^{n+1} - k_{s1}^{n+1}}{(n+1)(k_{s2} - k_{s1})}. \quad (17)$$

Since $\bar{k} = (k_{s1} + k_{s2})/2$ and assuming the approximate power law form for the true value of drag coefficient C_D (given in equation 6), we can approximate the percentage error due to use of the average hull roughness as

$$\frac{\% \Delta C_{D_{ahr}}}{100} = \frac{C_{D_{ahr}}}{C_D} - 1 = \frac{[\bar{k}]^n}{[k^n]} - 1 = \frac{(k_{s1} + k_{s2})^n (n+1)(k_{s2} - k_{s1})}{2^n (k_{s2}^{n+1} - k_{s1}^{n+1})}. \quad (18)$$

This expression explains the approximate behaviour seen in Fig. 5(b). Firstly, it is noted that the percentage error is zero if the exponent $n = 1$ (which is the only case where $[k^n] = [\bar{k}]^n$). This explains the fundamental shortcoming of computing the arithmetic mean (since Fig. 3 indicates that $n \neq 1$). Furthermore, equation (18) also shows that $\% \Delta C_{D_{ahr}} \rightarrow 0$ when $k_{s2} \rightarrow k_{s1}$, which for the current limits given in equation (14) will occur for the lowest Re_L and large L (small k_{s2}/L , lightest blue symbols on left hand side of x axis). Clearly the data exhibit this trend. Finally, when $k_{s2} \gg k_{s1}$, equation (18) suggests that $\% \Delta C_{D_{ahr}} \approx [(n+1)/2^n] - 1$, which for $n = 0.25$ assumed here suggests that $\% \Delta C_{D_{ahr}}$ will asymptote to ≈ 5 in the limit of large Re_L and/or large k_{s2}/L . This value is the maximum expected



Beta distribution

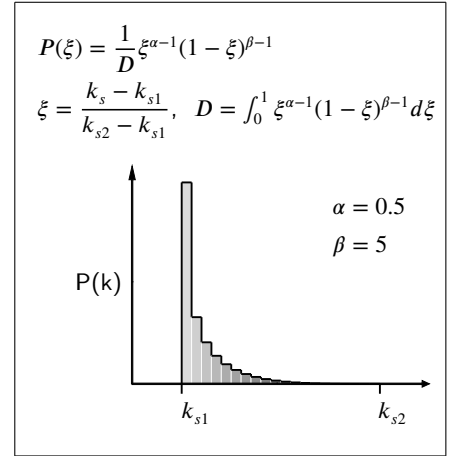


Figure 6: A flat plate of length L and width W , comprised of N strips of different roughness, where the strip width $S = W/N$. In this case the roughness length of each strip is taken from a beta distribution with $\alpha = 0.5$ and $\beta = 5$, leading to a greater probability of roughness strips at the small scale end of the range ($\rightarrow k_{s1}$).

error in predicted drag for a uniform distribution when the arithmetic mean k_{ahr} is used. The solid and dashed lines in Fig. 5(b) show the predicted error from equation (18) evaluated at $Re_L = 3 \times 10^7$ and $Re_L = 1 \times 10^{10}$. It is seen that these two curves approximately bound the computed behaviour in $\%C_{D_{ahr}}$ (blue shaded symbols) across the range of tested Re_L and k_{s2}/L . This suggests that the error in the drag estimate based on k_{ahr} can be reliably predicted if the roughness probability distribution function is known, without the need to invoke the boundary layer evolution methodologies outlined in Granville (1958); Monty et al. (2016); Pullin et al. (2017).

3.2. Different roughness distributions

The results presented in Fig. 5 are for the uniformly distributed roughness lengths (as illustrated in Fig. 4). Depending on the form of the distribution, the error for $C_{D_{ahr}}$ can be much larger. Fig. 6 shows a beta distribution with distribution.

$$P(\xi) = \frac{1}{D} \xi^{\alpha-1} (1-\xi)^{\beta-1} \quad (19)$$

where $\alpha = 0.5$, $\beta = 5$ and,

$$\xi = \frac{k_s - k_{s1}}{k_{s2} - k_{s1}}, \quad D = \int_0^1 \xi^{\alpha-1} (1-\xi)^{\beta-1} d\xi \quad (20)$$

In this case there is a higher probability of roughness patches close to the lower limit k_{s1} and a lower probability of patches with $k_s \rightarrow k_{s2}$. This scenario would represent a case where the hull was predominantly smooth (or with the baseline underlying coating roughness) with occasional patches of fouling. Fig. 7 shows the error in the drag penalty evaluated from (blue symbols) the power mean k_{ehr} and (grey symbols) the arithmetic mean k_{ahr} . In this case the error from assuming the arithmetic mean is much larger (tending to $\Delta C_{D_{ahr}} > 16\%$ in the high Re_L , high k_{s2}/L limit). Again, the power mean approximation performs well in minimising errors. The dot-dashed lines show that the error due to assuming $n = 0.25$ remains $< 1\%$ for $k_{s2}/L < 10^{-3}$. Based on the trend presented in Fig. 5(a), we might expect a lower exponent n to be optimal for this beta-distributed roughness, since $\overline{k_s}$ for the beta distribution is much less than that for the corresponding uniformly distributed case. Indeed, for the case presented, the error for the k_{ehr} predicted drag can be reduced to $< 0.5\%$ for $k_{s2}/L < 10^{-3}$ when $n = 0.23$.

In a similar manner to the analysis above for the uniform distribution, we can again assume that $\% \Delta C_{D_{ahr}} =$

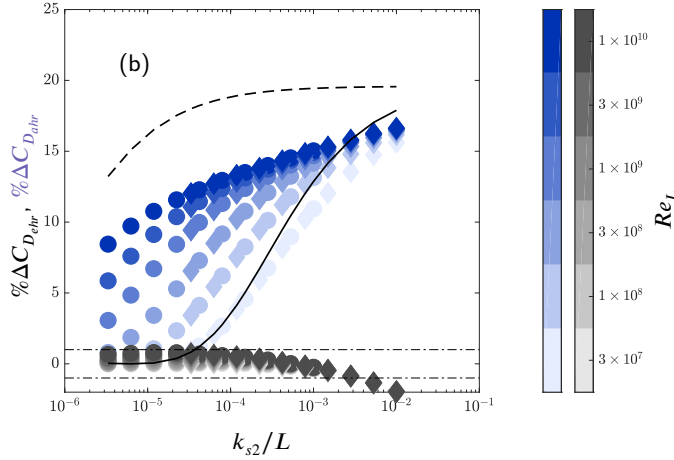


Figure 7: Error estimates for the beta probability distribution of roughness. (grey shaded symbols) show the percentage error between the drag predictions using the power mean k_{ehr} and the true estimate of the drag ($\Delta C_{D_{ehr}} = C_{D_{ehr}} - C_D$) and (blue shaded symbols) show the percentage error between the drag predictions using the arithmetic mean k_{ahr} and the true estimate of the drag ($\Delta C_{D_{ahr}} = C_{D_{ahr}} - C_D$). The (o) symbols show data with $k_{s2} = 0.001$ m and the (◇) symbols show $k_{s2} = 0.01$ m. The colour shading shows Re_L , with darkest shading showing highest Re_L (see colour scales on right-hand side). The dot-dashed lines show a $\pm 1\%$ margin, the solid and dashed lines show the predicted error from the PDF (equation 21) evaluated at $Re_L = 3 \times 10^7$ and $Re_L = 1 \times 10^{10}$.

$(\overline{[k]^n}/\overline{[k^n]}) - 1$, which for the beta distribution described in Fig. 6 yields,

$$\% \Delta C_{D_{ahr}} = \frac{[\overline{\xi(k_{s2} - k_{s1}) + k_{s1}}]^n}{[\overline{(\xi(k_{s2} - k_{s1}) + k_{s1})^n}]} - 1 \quad (21)$$

Evaluating equation (21) analytically requires the integration of the beta distribution PDF given in Fig. 6, which is non-trivial. However, in the limit of $k_{s2} \gg k_{s1}$ we can approximate (with some loss of accuracy) that $\% \Delta C_{D_{ahr}} \approx [\overline{\xi}]^n / [\overline{\xi^n}] - 1$. By evaluating the appropriately premultiplied PDFs between the limits of $0 < \xi < 1$ (for $\alpha = 0.5$ and $\beta = 5$) it can be shown that $[\overline{\xi}] = 256/(3465D)$ and $[\overline{\xi^n}] = 8192/(21945D)$ (for $n = 0.25$), with the normalisation constant D integrating to $256/315$. This crude analysis suggests that in the limit of high k_{s2}/L and high Re_L , the error will asymptote to 19.5%. The solid and dashed lines in Fig. 7 show the predicted error from the numerical solution of equation (21) at $Re_L = 3 \times 10^7$ and $Re_L = 1 \times 10^{10}$. It is once again seen that these two curves approximately bound the $\% \Delta C_{D_{ahr}}$ computed from the boundary layer evolution methodologies (blue shaded symbols) across the range of tested Re_L and k_{s2}/L (albeit with some over estimation).

4. Transitional roughness and the smooth limit

4.1. Cases where $Re_{k_s} \lesssim 150$

The solid bold line in Fig. 8(a) shows the assumed fully rough behaviour for ΔU^+ as a function of k_s^+ as given by equation (3). For all preceding analysis, this function has been exclusively used throughout and the lower limit of the roughness range has been set at $Re_{k_{s1}} = 150$, such that roughness patches in the assigned distributions predominantly lie within the fully rough regime (to the right of the black filled symbol in Fig. 8a). A re-analysis of Fig. 3 suggests that the power mean approach to ascribing an equivalent homogeneous roughness will fail when the lower limit k_{s1} is set below this value (to the left of the filled symbol in Fig. 8a), since only in the fully rough regime is C_D approximately proportional to $(k_s/L)^n$. To illustrate this, the solid bold line in Fig. 8(b) shows the corresponding drag coefficient curve for equation (3) as a function of k_s/L for a single illustrative Reynolds number $Re_L = 1 \times 10^8$. If $Re_{k_{s1}} \lesssim 150$, we would expect to be to the left of the filled symbol, where C_D will be invariant with k_s/L for a given Re_L , and hence any power law approximation will be challenged.

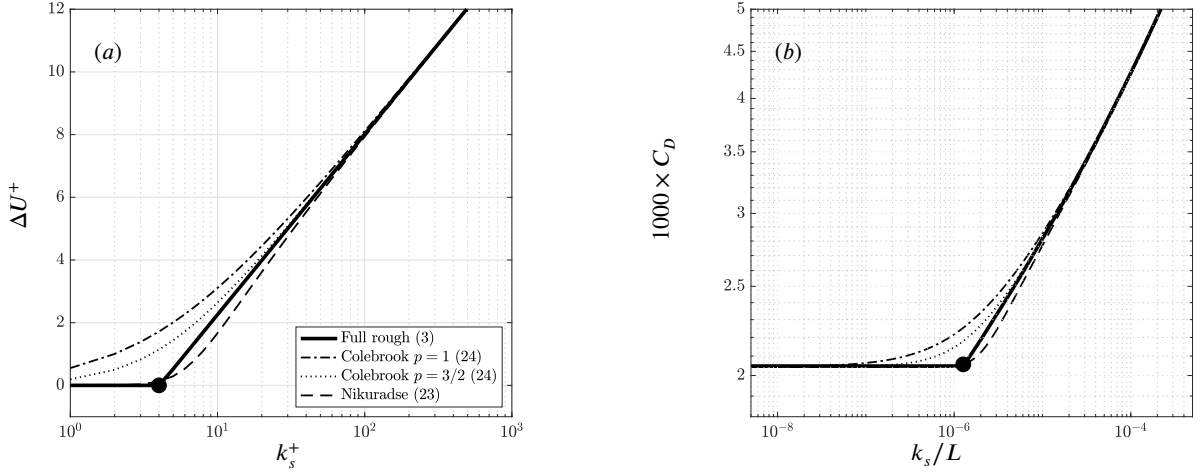


Figure 8: Different behaviour in the transitional regime. (a) Plots of the Hama roughness function $\Delta U^+(k_s^+)$ for (—) the fully rough function given in equation (3); (---) fit to Nikuradse's 1933 sandgrain roughness data given by equation (23); (---) and (---) generalised Colebrook-type formula with $p = 1$ and $p = 1.5$ respectively, as given by equation (24). (b) the corresponding drag coefficient curves as a function of k_s/L for $Re_L = 1 \times 10^8$.

Fig. 9(a) shows a comparison of the error in C_D computed from (grey symbols) the power mean k_{chr} and (blue symbols) the arithmetic mean k_{ahr} where $Re_{k_{s1}} = 0$. In this case we, simulate a beta roughness distribution ($\alpha = 0.5$, $\beta = 5$) with $k_{s1} = 0$, such that the roughness distribution now encroaches on the smooth and transitionally rough regime. As shown previously in Fig. 7, the arithmetic mean estimate causes larger errors in the computed drag. However, when the roughness distribution encroaches on the transitional regime, Fig. 9(a) shows that the error for the power mean approach (grey symbols) is now much greater for certain cases than that exhibited by the fully rough distributions in Fig. 7. This failure in the power mean approximation is expected, since the roughness distribution now extends into the transitional region (the horizontal black lines in Fig. 3 and Fig. 8b) where C_D is no longer solely a function of k_s/L , but also now depends on Reynolds number (Re_k or Re_L). Hence the approximate power law fit $C_D \propto (k_s/L)^n$ no longer holds. To further illustrate the source of this error, in Fig. 9(b) we isolate the error data at $Re_L = 1 \times 10^8$, and highlight with red vertical lines the mean roughness height (\bar{k}_s/L) for three different upper roughness limits ($k_{s2}/L = 1 \times 10^{-3}$, 3.3×10^{-5} and 3.3×10^{-6} , as shown by the dot-dashed, dashed and solid red lines respectively). Note that for the particular beta distribution considered here, $\bar{k}_s = k_{s2}/11$. In Fig. 9(c), the drag coefficient curve for the isolated Re_L case is replotted from Fig. 3. It is clear that the \bar{k}_s/L corresponding to the highest error in the power mean ($\approx 8\%$ error at $\bar{k}_s/L = 3 \times 10^{-6}$) in Fig. 9(b) corresponds closely to the location where the drag curve deviates from the fully rough behaviour in Fig. 9(c). Fig. 9(d) shows the premultiplied probability distribution function for the ascribed beta roughness distribution associated with the three highlighted values of k_{s2}/L . The maximum error corresponds to the case ($k_{s2}/L = 3.3 \times 10^{-5}$) where the roughness distribution strongly straddles the demarcation between smooth and fully rough behaviour. The accuracy of the power mean approach for cases where the distribution lies predominantly within the smooth region is relatively unaffected, with errors close to zero. This is expected, since equation (3) indicates that all data with $k_s^+ < e^{\kappa(B-A)}$ ($Re_k < O(150)$) will be set to $\Delta U^+ = 0$, which is equivalent to setting all roughness in the smooth regime equal to $k_s^+ = e^{\kappa(B-A)}$. Conversely, when the roughness distribution is predominantly located within the fully rough regime, the previous analysis in § 3.2 indicates that the error for the power mean approach remains low. To reiterate this finding, Fig. 9(e) presents the error data from Fig. 9(a) as a function of $Re_{k_s}^- (\equiv U_\infty \bar{k}_s/\nu)$. Presented in this way, it is clear that the maximum error corresponds to $Re_{k_s}^- = O(150)$ corresponding to the case where the roughness distribution straddles the fully rough and smooth regimes.

By way of a solution, and based on the analysis in Fig. 9, we can propose a modification to the power mean approach where all roughness in the distribution below the smooth limit of $Re_{k_s} = O(125)$ are set to the smooth limit

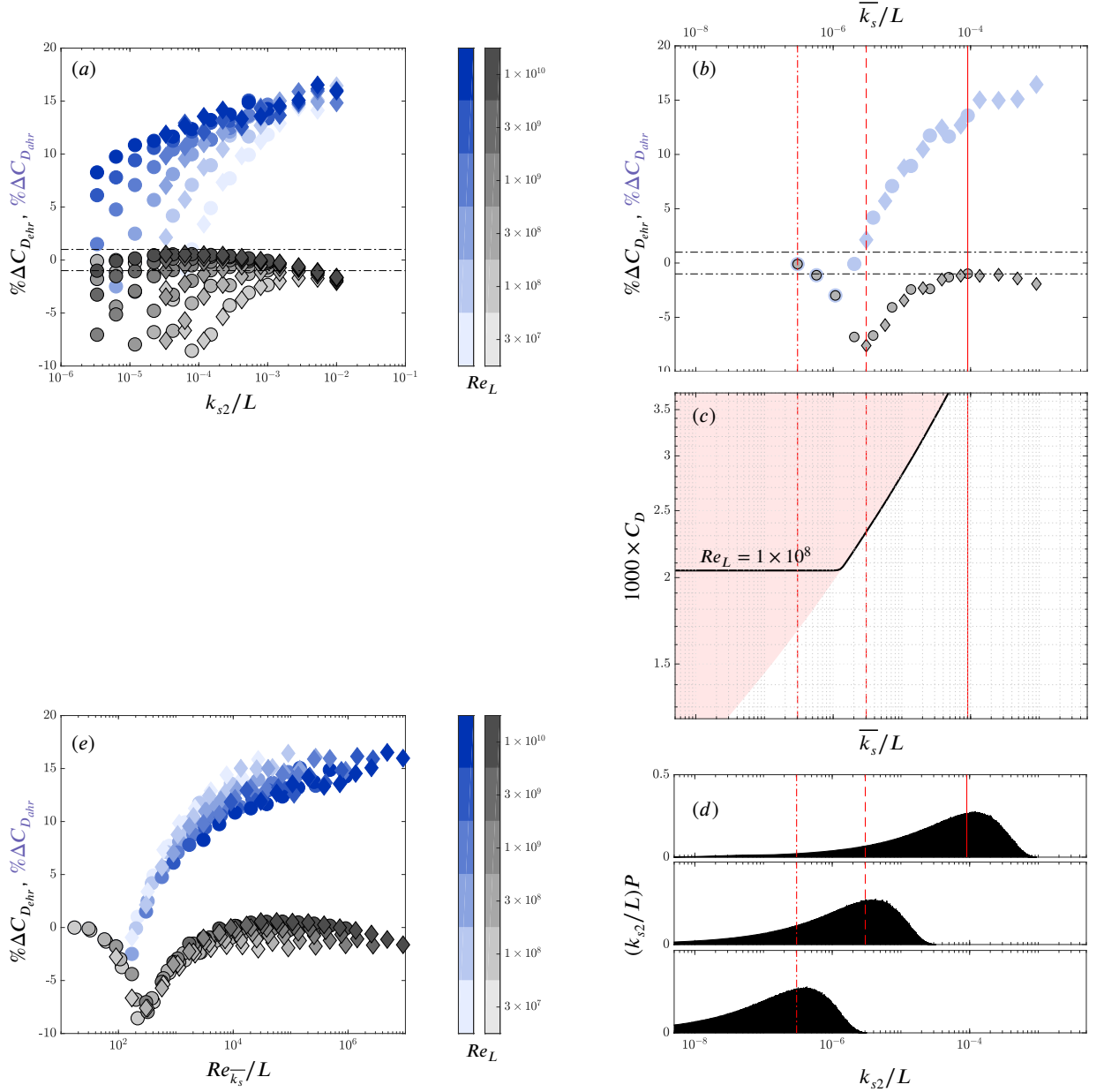


Figure 9: The transitionally rough case. (a) Error estimates from different averaging approaches where the lower limit of the roughness range is within the transitional regime ($k_{s1} = 0$). (grey shaded symbols) show the percentage error between the drag predictions using the power mean k_{ehr} and the true estimate of the drag ($\Delta C_{D_{ehr}} = C_{D_{ehr}} - C_D$) and (blue shaded symbols) show the percentage error between the drag predictions using the arithmetic mean k_{ahr} and the true estimate of the drag ($\Delta C_{D_{ahr}} = C_{D_{ahr}} - C_D$). The (o) symbols show data with $k_{s2} = 0.001$ m and the (\diamond) symbols show $k_{s2} = 0.01$ m. The colour shading shows Re_L , with darkest shading showing highest Re_L (see colour scales on right-hand side). In plot (b) we isolate the case where $Re_L = 1 \times 10^8$ and L is logarithmically varied from $1 < L < 300$ m. The data in this figure are plotted against $\overline{k_s}/L$, which is the mean of the assigned beta distribution. (c) shows the corresponding curve of C_D against $\overline{k_s}/L$. The three vertical red lines denote 3 illustrative cases of $\overline{k_s}/L$ for distributions with the upper roughness bound set to (—) $k_{s2}/L = 1 \times 10^{-3}$, (- -) 3.3×10^{-5} and (-.-) 3.3×10^{-6} . (c) shows the corresponding premultiplied roughness probability distributions for these three cases. (e) shows the same data as plot (a) but replotted in terms of $Re_{k_{s2}}$.

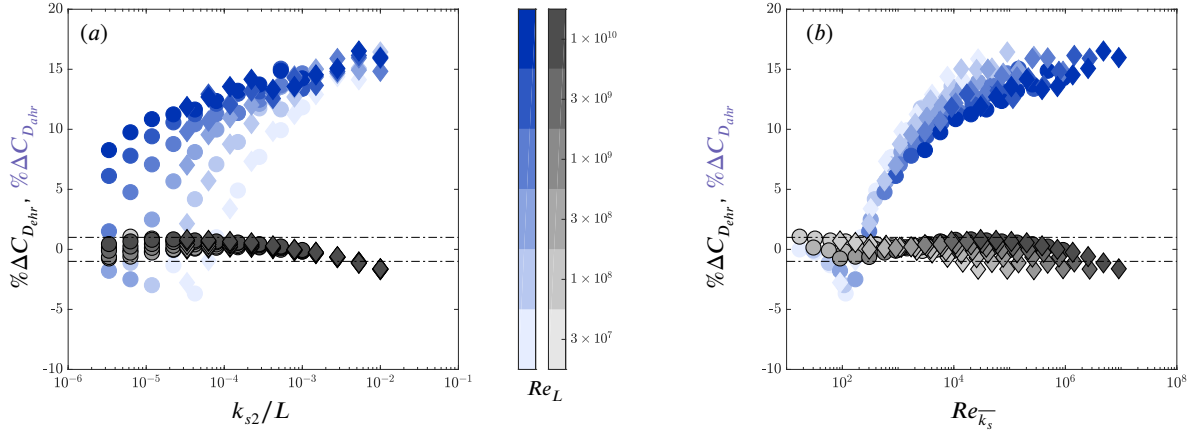


Figure 10: The modified transitionally rough case using the power mean averaging described in equation (22). Error estimates from different averaging approaches where the lower limit of the roughness range is within the transitional regime ($k_{s1} = 0$). (grey shaded symbols) show the percentage error between the drag predictions using the power mean k_{ehr} and the true estimate of the drag ($\Delta C_{D_{ehr}} = C_{D_{ehr}} - C_D$) and (blue shaded symbols) show the percentage error between the drag predictions using the arithmetic mean k_{ahr} and the true estimate of the drag ($\Delta C_{D_{ahr}} = C_{D_{ahr}} - C_D$). The (o) symbols show data with $k_{s2} = 0.001$ m and the (◇) symbols show $k_{s2} = 0.01$ m. The colour shading shows Re_L , with darkest shading showing highest Re_L (see colour scales on right-hand side). In plot (a) errors are plotted against k_{s2}/L , while in plot (b) we plot the same data against $Re_{k_s}^-$.

$$(k_s \approx 125L/Re_L),$$

$$k_{ehr} = \left[\frac{1}{A} \sum_{i=1}^N k_{si}^n A_i \right]^{\frac{1}{n}} \quad k_{si} = \begin{cases} k_{si}, & \text{if } Re_{k_{si}} > 125 \\ \frac{125L}{Re_L}, & \text{otherwise} \end{cases} \quad (22)$$

Fig. 10(a) and (b) plot the same cases as Fig. 9(a) and (e) but with the modified definition for k_{ehr} given in equation (22). This refinement is effective in correcting the previously identified error in the transitional regime. In Fig. 10(b) where the error data are plotted against $Re_{k_s}^-$ we see that the modified power mean approach has remedied all of the error noted in Fig. 9(e) at the location of the smooth limit. It is noted that this refinement is only required for distributions that are heavily skewed towards k_{s1} . For example, even with $k_{s1} = 0$, and without the refinement suggested in equation (22), the uniform distribution yields an error in drag prediction $\% \Delta C_{D_{ehr}}$ for the power mean that is everywhere $< 1\%$. However, due to the simplicity of implementation, we adopt this refined definition of $k_{s_{ehr}}$ for all remaining analysis.

4.2. Different $\Delta U^+(k_s^+)$ behaviour in the transitional regime

We might also consider the cases where the roughness function follows a different distribution in the transitionally rough regime. We here consider Nikuradse-type and Colebrook distributions as described in equations (23) and (24). Two different values for p are considered for the Colebrook distribution, with $p = 1$ corresponding to the original form (see for example Schultz, 2004; Grigson, 1992).

Nikuradse

$$\Delta U^+ = \frac{1}{p\kappa} \log(1 + \beta(k_s^+)^p) \quad \beta = \exp(p\kappa [A - B - (C/k_s^+)^D]) \quad \begin{cases} p = 2.5 \\ C = 8 \\ D = 1 \end{cases} \quad (23)$$

Generalised Colebrook

$$\Delta U^+ = \frac{1}{p\kappa} \log(1 + \beta(k_s^+)^p) \quad \beta = \exp(p\kappa [A - B]) \quad \begin{cases} p = 1 \text{ or} \\ p = 3/2 \end{cases} \quad (24)$$

These distributions are based on the generalised roughness function of Cheng, Pullin and Samtaney (2020), all of which asymptote to the fully rough curve ($\Delta U^+ = \kappa^{-1} \log k_s^+ + A - B$) in the limit of $k_s^+ \gg 1$. The dashed, dot-dashed and dotted lines in Fig. 8(a) show the roughness functions for these different transitional behaviours, along with the corresponding drag coefficient curves $C_D(k_s/L)$ in Fig. 8(b). Compared with the fully rough behaviour assumed up to this point (shown by the bold lines in Fig. 8 and given by equation 3), we might expect these alternative transitionally rough behaviours to reduce the accuracy of the power mean approach in the transitional regime since the assumption that the $C_D \propto (k_s/L)^n$ will be increasingly violated, especially for the Colebrook-type behaviours.

To quantify this problem, Fig. 11 plots the error in the predicted drag coefficient C_D for (grey symbols) the power mean k_{ehr} and (blue symbols) the arithmetic mean k_{ahr} approaches, for the beta distribution with $k_{s1} = 0$ and with the different transitionally rough models. Fig. 11(a,b) show results for the Nikuradse-type profile (equation 23). A comparison of these plots with Fig. 10 indicates a diminished accuracy of the power mean approach for the Nikuradse roughness function as compared to the previously assumed fully rough behaviour (equation 3). It is clear from Fig. 11(b) that this error is centred around $Re_{\bar{k}_s} \approx 300$, which matches the point in Fig. 8(b) where the maximum deviation occurs between the Nikuradse and fully-rough models (for the case shown in Fig. 8b with $Re_L = 1 \times 10^8$, maximum deviation between the solid and dashed lines occurs at $k_s/L \approx 3 \times 10^{-6}$ which corresponds to $Re_{k_s} \approx 300$). For the Nikuradse formulation, the error caused by the power mean approach is $< 2.5\%$. As discussed below, such errors only occur when the mean observed roughness height is close to the smooth limit (which is only likely to occur for freshly recoated vessels). For the Colebrook-type behaviours shown in Fig. 11 (c-f), the power mean approach leads to an over estimation of the drag in the transitional regime. This error exceeds 1% becoming progressively worse for $Re_{\bar{k}_s} \lesssim 200$, and the maximum error is greater for the $p = 1$ Colebrook than for $p = 3/2$. For $Re_{\bar{k}_s} \lesssim 200$ the error due to the power mean (gray symbols) becomes greater than the error due to the arithmetic mean approach (blue symbols) for the beta distribution. Together the results in Fig. 11 suggest that the power mean approach still works remarkably well for surfaces with a Colebrook or Nikuradse type behaviour, provided that the mean roughness height of the roughness distribution is beyond the transitional limit. For cases where the mean height is transitional or sub-transitional ($Re_{\bar{k}_s} \lesssim 200$) the advantage of the power mean approach for beta distributions diminishes, and indeed for Colebrook type surfaces a traditional arithmetic mean performs better than the power mean where $Re_{\bar{k}_s} \lesssim 200$. Note that for this beta distribution, $Re_{\bar{k}_s} = 200$ suggests that $Re_{k_{s2}} = 2200$ (since $\bar{k}_s = k_{s2}/11$ for $\alpha = 0.5$ and $\beta = 5$). To put this into perspective, for the frigate considered by Schultz (2007) at $U_\infty = 7.71 \text{ ms}^{-1}$, this corresponds to $\bar{k}_s \approx 23\mu\text{m}$ and $k_{s2} \approx 256\mu\text{m}$. This likely represents an unusually smooth hull, with a mean roughness height which is less than that suggested by Schultz (2007) for an ‘as applied anti-fouling coating’ and with less than 3% of the surface exhibiting roughness where $k_s > 100\mu\text{m}$ (‘deteriorated coating or light slime’ Schultz, 2007). It should also be noted that the errors shown for k_{ehr} by the grey symbols in Fig. 11 are symptomatic of the highly skewed beta distribution. For a uniform distribution, shown by the red shaded symbols in Fig. 11, errors in the power mean for the three tested roughness models are $< 1.5\%$ for all $Re_{\bar{k}_s} \gtrsim 200$ and $k_{s2}/L \lesssim 10^{-3}$ (a range that is likely representative of most realistic ship operations). Again, using the example of the frigate presented by Schultz (2007), $Re_{\bar{k}_s} = 200$ corresponds to a case where the maximum roughness size $k_{s2} = 2\bar{k}_s \approx 46\mu\text{m}$; a maximum roughness height between that listed by Schultz (2007) for ‘as applied anti-fouling coating’ and ‘deteriorated coating or light slime’. It is fair to assume then, that for most operating conditions, even when transitionally rough surfaces are present, the power mean approach will retain its superior performance.

5. Remaining Issues

The following issues persist for the averaging procedure outlined here. In many cases further investigations will be required to address these.

Equivalent sandgrain roughness k_s . The power mean average relies on the ability to ascribe an equivalent sandgrain roughness k_s to each heterogeneous patch. Despite recent progress in correlations that relate k_s to topography (see Chung et al., 2021; Flack and Chung, 2022), this remains a substantial source of error in the averaging procedure and one that is not accounted for here.

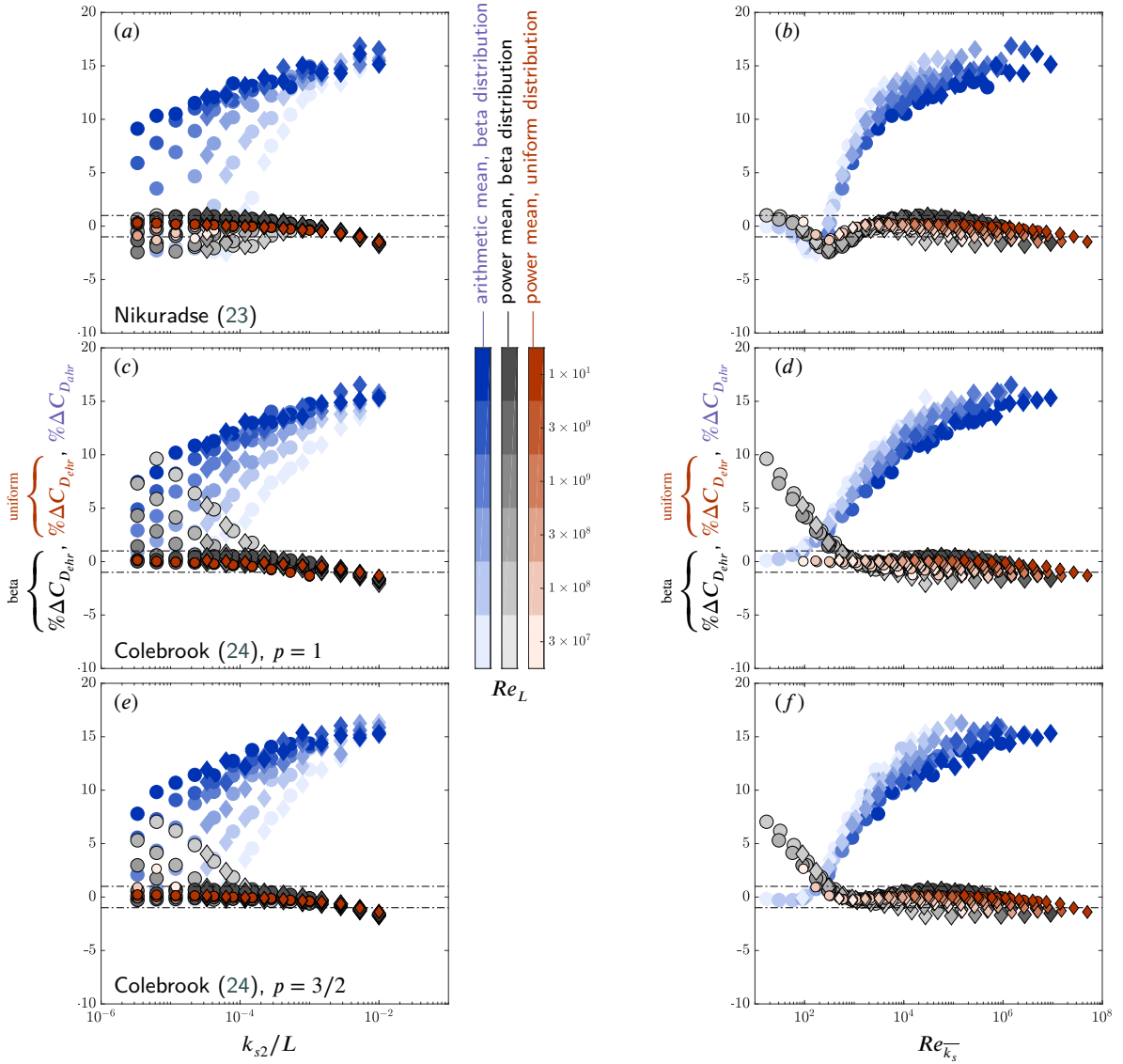


Figure 11: The effect of different transitional fits for $\Delta U^+(k_s^+)$ on the error estimates from different averaging approaches. (a,b) Nikuradse's 1933 sandgrain roughness data given by equation (23); (c,d) generalised Colebrook-type formula with $p = 1$ as given by equation (24); (e,f) generalised Colebrook-type formula with $p = 3/2$ as given by equation (24). (grey shaded symbols) show the percentage error between the drag predictions using the power mean k_{ehr} and the true estimate of the drag ($\Delta C_{D_{ehr}} = C_{D_{ehr}} - C_D$) for the beta distribution with $\alpha = 0.5$, $\beta = 5$ and $k_{s1} = 0$. (red shaded symbols) show the corresponding percentage error for the power mean for the uniform distribution. The modified transitionally rough power mean averaging described in equation (22) is used. (blue shaded symbols) show the percentage error between the drag predictions using the arithmetic mean k_{ahr} and the true estimate of the drag ($\Delta C_{D_{ahr}} = C_{D_{ahr}} - C_D$). The (o) symbols show data with $k_{s2} = 0.001$ m and the (\diamond) symbols show $k_{s2} = 0.01$ m. The colour shading shows Re_L , with darkest shading showing highest Re_L (see colour scales on right-hand side). In left-hand column, errors are plotted against k_{s2}/L , while in right-hand column the same data are plotted against $Re_{k_s}^-$.

Relative position of heterogeneous patches on the hull. No attempt is made here to account for position of patches along the hull. In fact all heterogeneous patches considered are spanwise strips extending the full length of the vessel. It is reasonable to expect that roughness towards the bow may have a higher drag (or higher weighting) due to the thinner local boundary layers and higher local C_f (as indeed is shown by Suastika et al., 2021; Song et al., 2021). Likewise, patches towards the stern would have diminished contribution to drag as the hull approaches the smooth plate limit (see Pullin et al., 2017). In the future, it may be the case that a measure of streamwise patch location \hat{x} could be incorporated into the power mean approach (perhaps as a weighting parameter, or as a normalising lengthscale for k).

Equilibrium assumption. It is here assumed that the flow above the patches can be predominantly assumed to be in local equilibrium with the surface condition. This equilibrium assumption is implicit in the methods of Granville (1958); Monty et al. (2016); Pullin et al. (2017) that are used here for predicting C_D . Such assumptions are only approximately valid where the heterogeneous patch area $\gg \delta$. Future testing is required to determine the smallest patch sizes that still admit the power mean approach. Future high fidelity experiments or numerical simulations over heterogeneous plates or hull geometries, with resolved non-equilibrium behaviour (secondary flows and internal layers) will be required to fully validate the power mean approach.

The appropriate roughness distribution. As shown in § 3.2, the advantage of the power mean approach over methods that use an arithmetic mean is dependent on the distribution of the heterogeneous roughness distribution. The error due to assuming an arithmetic mean is much more pronounced for a skewed beta type distribution than for uniform distributions. Likewise, inaccuracies in the power mean caused by the roughness model in the transitional regime are much more pronounced for the beta distribution. In the future it would be useful to document the roughness distributions that are most commonly observed for heterogeneously fouled operating vessels. This will have implications for the optimal averaging scheme.

6. Conclusions

Based on assumed equilibrium behaviour for turbulent boundary layers developing over heterogeneous roughness, it is demonstrated that the power mean averaging approach can provide a reliable estimate for an equivalent homogeneous roughness length. The optimal exponent n for the power mean is a weak function of roughness distribution and ship operating conditions and it is found that $n = 0.25$ yields power mean errors $< 1\%$ for most realistic scenarios. For fully rough heterogeneous distributions, the power mean performs better than the arithmetic mean approaches that seem to be common place in the shipping industry. It is shown that the degree of error for the arithmetic mean is a function of the distribution of the heterogeneous roughness patches. For uniform distributions, with realistic upper and lower roughness limits and for realistic ship operating conditions, the likely error in C_D due to an equivalent homogeneous roughness computed from the arithmetic mean is $< 4\%$. However, for a beta distribution (with $\alpha = 0.5$ and $\beta = 5$) such errors can increase to approximately 16% . For both distributions it is shown that the power mean estimate remains accurate to within 1% . For beta type heterogeneous distributions, with lower roughness limits that encroach into the transitionally rough regime or smooth limit, the power mean approach must be modified such that all observed roughness with $Re_k < 125$ are resized in the averaging procedure as $k_{si} = 125L/Re_L$. It is shown that the error with the power mean approach for beta distributions can increase to a maximum of 2.5% where Nikuradse transitional models are assumed and when the mean roughness height is close to the transitional limit ($Re_k^- \gtrsim 300$). For Colebrook transitional models with a beta roughness distribution, the arithmetic mean approach becomes more accurate than the power mean for $Re_k^- \lesssim 200$. For uniform distributions, the error for the power mean estimate k_{ehr} remains less than 1.5% for both Nikuradse or Colebrook models where $Re_k^- \gtrsim 200$.

There remain outstanding questions regarding the equilibrium assumption used in the analysis here, and in appropriately accounting for the streamwise location of the roughness patches. Since the analysis shows that the accuracy of the power mean approach (and indeed the inaccuracy of the arithmetic mean approach) is dependant on roughness distribution, a database of realistic heterogeneous distributions observed in practise would permit a useful extension of this analysis.

References

- Antonia, R.A., Luxton, R.E., 1971. The response of a turbulent boundary layer to a step change in surface roughness. Part 1. Smooth to rough. *J. Fluid Mech.* 48, 721–761.

- Antonia, R.A., Luxton, R.E., 1972. The response of a turbulent boundary layer to a step change in surface roughness. Part 2. Rough to smooth. *J. Fluid Mech.* 53, 737–757.
- Bou-Zeid, E., Meneveau, C., Parlange, M.B., 2004. Large-eddy simulation of neutral atmospheric boundary layer flow over heterogeneous surfaces: Blending height and effective surface roughness. *Water Resour. Res.* 40, W02505.
- Busse, A., Jelly, T.O., 2020. Influence of surface anisotropy on turbulent flow over irregular roughness. *Flow Turbul. Combust.* 104, 331–354.
- Chan, L., MacDonald, M., Chung, D., Hutchins, N., Ooi, A., 2015. A systematic investigation of roughness height and wavelength in turbulent pipe flow in the transitionally rough regime. *J. Fluid Mech.* 771, 743–777.
- Cheng, W., Pullin, D.I., Samtaney, R., 2020. Large-eddy simulation and modelling of Taylor–Couette flow. *Journal of Fluid Mechanics* 890.
- Chung, D., Hutchins, N., Schultz, M.P., Flack, K.A., 2021. Predicting the drag of rough surfaces. *Annu. Rev. Fluid Mech.* 53, 439–471.
- Chung, D., Monty, J.P., Hutchins, N., 2018. Similarity and structure of wall turbulence with lateral wall shear stress variations. *J. Fluid Mech.* 847, 591–613.
- Flack, K., Chung, D., 2022. Important Parameters for a Predictive Model of k_s for Zero Pressure Gradient Flows.
- Flack, K.A., Schultz, M.P., 2010. Review of hydraulic roughness scales in the fully rough regime. *J. Fluids Engng.* 132, 041203.
- Flack, K.A., Schultz, M.P., Barros, J.M., 2020. Skin friction measurements of systematically-varied roughness: probing the role of roughness height and skewness. *Flow Turb. Combust.* 104, 317–329.
- Granville, P.S., 1958. The frictional resistance and turbulent boundary layer of rough surfaces. Technical Report 1024. David Taylor Model Basin.
- Grigson, C., 1992. Drag losses of new ships caused by hull finish. *J. Ship Res.* 31, 70–77.
- Hanson, R.E., Ganapathisubramani, B., 2016. Development of turbulent boundary layers past a step change in wall roughness. *J. Fluid Mech.* 795, 494–523.
- Hinze, J.O., 1967. Secondary currents in wall turbulence. *Phys. Fluids* 10, S122.
- International Paints, 2004. Hull roughness penalty calculator. Technical Report. International Paints.
- Jelly, T.O., Busse, A., 2018. Reynolds and dispersive shear stress contributions above highly skewed roughness. *J. Fluid Mech.* 852, 710–724.
- Li, M., de Silva, C.M., Chung, D., Pullin, D., Marusic, I., Hutchins, N., 2021. Experimental study of a turbulent boundary layer with a rough-to-smooth change in surface conditions at high Reynolds numbers. *J. Fluid Mech.* 923, A18.
- Macdonald, R.W., Griffiths, R.F., Hall, D.J., 1998. An improved method for the estimation of surface roughness of obstacle arrays. *Atmos. Environ.* 32(11), 1857–1864.
- Medjnoun, T., Vanderwel, C., Ganapathisubramani, B., 2018. Characteristics of turbulent boundary layers over smooth surfaces with spanwise heterogeneities. *J. Fluid Mech.* 838, 516–543.
- Monty, J.P., Dogan, E., Hanson, R., Scardino, A.J., Ganapathisubramani, B., Hutchins, N., 2016. An assessment of the ship drag penalty arising from light calcareous tubeworm fouling. *Biofouling* 32, 451–464.
- Napoli, E., Armenio, V., De Marchis, M., 2008. The effect of the slope of irregularly distributed roughness elements on turbulent wall-bounded flows. *J. Fluid Mech.* 613, 385–394.
- Naval Ships' Technical Manual, 2006. Marine fouling and its prevention. Technical Report Chapter 081. Naval Sea Systems Command, Washington (DC). Publication Number: S9086-CQ-STM-010/CH-081 Revision 5.
- Nikuradse, J., 1933. Laws of flow in rough pipes. Technical Report Technical Memorandum 1292. NACA. Translation from German published 1950.
- Placidi, M., Ganapathisubramani, B., 2015. Effects of frontal and plan solidities on aerodynamic parameters and the roughness sublayer in turbulent boundary layers. *J. Fluid Mech.* 782, 541–566.
- Prandtl, L., Schlichting, H., 1934. The resistance law for rough plates. Technical Report Translation 258. David W. Taylor Model Basin. Translation from German published 1955.
- Pullin, D., Hutchins, N., Chung, D.C., 2017. Turbulent flow over a long flat plate with uniform roughness. *Phys. Rev. Fluids* 2, 082601.
- Raupach, M.R., Antonia, R.A., Rajagopalan, S., 1991. Rough-wall turbulent boundary layers. *Appl. Mech. Rev.* 44, 1–25.
- Rouhi, A., Chung, D., Hutchins, N., 2019. Direct numerical simulation of open-channel flow over smooth-to-rough and rough-to-smooth step changes. *J. Fluid Mech.* 866, 450–486.
- Saito, N., Pullin, D.I., 2014. Large eddy simulation of smooth?rough?smooth transitions in turbulent channel flows. *Int. J. Heat Fluid Flow* 78, 707–720.
- Schlichting, H., 1936. Experimental investigation of the problem of surface roughness. Technical Report Technical Memorandum 823. NACA. Translation from German published 1937.
- Schultz, M.P., 2004. Frictional resistance of antifouling coating systems. *J. Fluids Engng.* 126, 1039–1047.
- Schultz, M.P., 2007. Effects of coating roughness and biofouling on ship resistance and powering. *Biofouling* 23, 331–341.
- Song, S., Ravenna, R., Dai, S., DeMarco Muscat-Fenech, C., Tani, G., Demirel, Y.K., Atlar, M., Day, S., Incecik, A., 2021. Experimental investigation on the effect of heterogeneous hull roughness on ship resistance. *Ocean Engineering* 223, 108590.
- Suastika, I., Hakim, M., Nugroho, B., Nasirudin, A., Utama, I., Monty, J., Ganapathisubramani, B., 2021. Characteristics of drag due to streamwise inhomogeneous roughness. *Ocean Engineering* 223, 108632.
- Taylor, P.A., 1987. Comments and further analysis on effective roughness lengths for use in numerical three-dimensional models. *Boundary-Layer Meteorol.* 39, 403–418.
- Thakkar, M., Busse, A., Sandham, N.D., 2017. Surface correlations of hydrodynamic drag for transitionally rough engineering surfaces. *J. Turbul.* 18, 138–169.
- Townsend, A.A., 1976. The Structure of Turbulent Shear Flow. Second ed., Cambridge University Press.
- Wangawijaya, D.D., Baidya, R., Chung, D., Marusic, I., Hutchins, N., 2020. The effect of spanwise wavelength of surface heterogeneity on turbulent secondary flows. *J. Fluid Mech.* 894, A7.
- Yang, J., Anderson, W., 2018. Numerical study of turbulent channel flow over surfaces with variable spanwise heterogeneities: topographically-driven secondary flows affect outer-layer similarity of turbulent length scales. *Flow Turbul. Combust.* 100, 1–17.